Published in Physical Chemistry, Chemical Physics (PCCP) 8, 513 - 520, 2006
which should be used for any reference to this work

Adsorption kinetics of L-glutathione on gold and structural changes during self-assembly: an *in situ* ATR-IR and QCM study

Marco Bieri and Thomas Burgi*

The adsorption of L-glutathione (γ-Glu-Cys-Gly) from ethanol on gold surfaces was studied *in situ* by both attenuated total reflection infrared (ATR-IR) spectroscopy and using a quartz crystal microbalance (QCM). The molecule is firmly anchored to the gold surface through the thiol group. Different IR signals of adsorbed L-glutathione, notably the amide I and ν(–COOH), show significantly different behavior with time, which reveals that their increase is not related to adsorption (mass uptake) alone. This indicates that structural transformations take place during the formation of the self-assembled monolayer (SAM). In particular, the intensity of the acid signal increases quickly only within the first couple of minutes. The complexity of the self-assembling process is confirmed by QCM measurements, which show fast mass uptake within about 100 s followed by a considerably slower regime. The structural change superimposed on the mass uptake is, based on the *in situ* time-resolved ATR-IR measurements, assigned to the interaction of the acid group of the Gly moiety with the surface. The latter group is protonated in ethanol but deprotonates upon interaction with the gold surface. The protonation–deprotonation equilibrium is sensitive to external stimuli, such as the presence of dissolved L-glutathione molecules. The interaction of the acid group with the surface and concomitant deprotonation proceeds *via* two distinguishable steps, the first being a reorientation of the molecule, followed by the deprotonation.

Introduction

Self-assembled monolayers (SAMs) have been extensively studied in recent years[1–3] due to their potential applications in various branches of surface technology, such as passivation, lubrication, surface engineering, development of (bio-)sensors[4] and biocompatibility. The self-assembly of alkanethiols on gold surfaces was the focus of many studies due to the model character of this system. However, even for these simple models relatively complex adsorption behavior was found, deviating from Langmuir adsorption. Despite the fact that some central assumptions of the Langmuir model are not met (no intermolecular interactions, the adsorption probability only determined by the available free sites), deviations are expected due to the rich phase diagram of these systems.[5] At very low coverage the adsorbed molecules lay flat on the surface, whereas at high coverage a standing structure is formed with the individual molecules tilted with respect to the surface. At intermediate coverage still more phases were found. Therefore, as coverage increases, the system crosses phase boundaries. The different phases have their own energy landscape and thus adsorption kinetics can be heavily affected when crossing phase boundaries.[3] For more complicated thiols with additional functional groups the phase diagram (in temperature and coverage) is not expected to become simpler. Indeed, rather complex phase diagrams were found for relatively small molecules such as tartaric acid adsorbed on metal surfaces.[6]

An important class of SAMs is those composed of polypeptides containing cysteine. These molecules contain other functional groups besides thiol which may also interact with the surface[7] and give rise to intra- and intermolecular interactions. This has important consequences on the properties of the corresponding SAM but is also likely to be important for the self-assembling process itself. In this contribution we focus on the self-assembly of L-glutathione (GSH, γ-Glu-Cys-Gly, Scheme 1) on gold. GSH has various physiological functions and is the most abundant non-protein thiol in mammalian cells.[8] GSH-modified gold surfaces were considered for specific protein binding.[9] Furthermore, GSH SAMs on gold electrodes exhibited "ion gating" when interacting with rare earth metal ions, transition metal ions, neurotransmitters and a cationic drug. Interaction with these analytes opened up free electrode surface as revealed by redox ion probes.[10,11]The adsorbed molecules also respond with significant structural changes towards acid–base stimuli.[12] It was found that the acid group

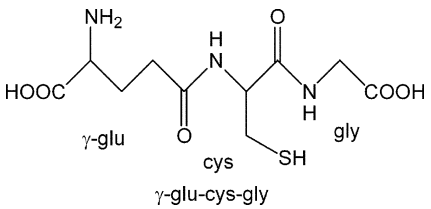

Scheme 1 Structure of L-glutathione (GSH, γ-Glu-Cys-Gly).

Université de Neuchâtel, Institut de Chimie, Rue Emile-Argand 11, 2007 Neuchâtel, Switzerland. E-mail: thomas.burgi@unine.ch; Fax: ++41 32 718 25 11; Tel: ++41 32 718 24 12

of the Gly can interact with the gold surface.[12] In the following it will be shown by using a combination of *in situ* attenuated total reflection infrared (ATR-IR) spectroscopy[13] and quartz crystal microbalance (QCM) measurements [14] that the relative complexity of GSH with its flexible structure and presence of ionizable functional groups is reflected in its self-assembly and adsorption kinetics. The ATR-IR spectra shed light onto the structural changes which are at the origin of the complex adsorption behavior.

Experimental

Chemicals

L-glutathione (γ-Glu-Cys-Gly, GSH, Sigma Aldrich Inc., ≥ 98%) was used as received. Ethanol (EtOH, Merck p.a.) served as the solvent for both the ATR-IR and QCM measurements reported here.

In situ ATR-IR spectroscopy

Sample preparation. ATR-IR measurements were performed using a Ge internal reflection element (IRE, 50 mm × 20 mm × 2 mm, Komlas). The IRE was first polished with a 0.25 μm grain size diamond paste (Buehler, Metadi II) and rinsed copiously with EtOH before the surface was plasma cleaned under a flow of air for 5 min. In the next step, a gold layer with a thickness of about 2 nm was sputtered onto the IRE. It should be noted that sputtering of such thin films does not result in uniformly flat gold surfaces but rather islands or particles (see for example ref. 15). A freshly prepared IRE was used for each ATR-IR experiment. In control experiments using a bare Ge IRE the absence of prominent GSH signals revealed no GSH adsorption during several hours of exposure to GSH solution.

Data acquisition. A Bruker EQUINOX 55 FT-IR spectrometer equipped with a nitrogen cooled narrow band MCT detector was used for ATR-IR measurements. The spectral resolution used for all experiments was 4 cm^{-1}. The Ge IRE was mounted on a home-built liquid flow-through cell (0.077 mL volume) with a gap of 250 μm between the IRE and the polished steel surface. The flow-through cell can be heated or cooled but all measurements reported here were performed at room temperature. More detailed descriptions of the flow-through cell can be found elsewhere.[16,17]

ATR-IR experiments. The solvent (EtOH) and GSH solution (typically 0.33 mM for ATR-IR experiments) were stored in separate bubble tanks. Before starting an experiment both the solvent and GSH solution were saturated with nitrogen gas (CarbaGas, 99.995%). An experiment started with a flow of EtOH over the gold coated Ge IRE until no variation in the spectrum could be detected (about 5 min). Then a spectrum was recorded by co-adding 200 interferograms which served as a reference for all subsequent measurements. Two types of ATR-IR experiments were carried out: in the first experiment GSH was flowed (flow rate = 0.18 mL min^{-1}) over the gold coated Ge IRE for more than 4 h and the spectral changes were followed. Spectra were recorded by co-adding 200 interferograms at a 40 kHz sampling rate resulting in time intervals of 42 s between subsequent spectra. The time-dependence of the bands in the ATR-IR spectra yields information on the velocity of adsorption and structural changes occurring during the GSH self-assembling process. The second type of ATR-IR experiment is identical to that described above, except that adsorption of GSH was stopped after some time by replacing the flow of GSH solution with solvent (EtOH). This abrupt stop of GSH supply may have an impact on the GSH SAM structure; possible scenarios are the desorption of adsorbed molecules or restructuring of the adsorbate layer. To adequately follow the changes in the spectra the rapid scan acquisition mode of the FT-IR spectrometer was used resulting in time intervals down to 20 s. Note that with the use of small GSH concentrations (0.33 mM) contributions from bulk molecules can be neglected, as was verified in control experiments with the bare Ge IRE.

Quartz crystal microbalance

Instrumentation. QCM measurements were performed with a QCM200 model (Stanford Research Systems) with a 5 MHz (nominal) crystal oscillator. The sensor crystals (5 MHz, AT cut, 1 in diameter, Stanford Research Systems) are a chrome–gold composite with an optically clear surface finish (about 50 nm average surface roughness). The QCM is operated with an axial flow cell (Stanford Research Systems) providing high sensitivity and well defined flow conditions. In the axial flow cell of about 150 μL volume, the sample flows radially outward from the input port at the center of the cell to the exit channel at the edge of the cell. The sample solution is injected perpendicularly with respect to the flat surface of the QCM crystal. The stagnation point is located at the center of the crystal, overlapping the area of highest sensitivity of the flat QCM oscillator. Information about the hydrodynamics associated with stagnation point flow can be found elsewhere.[18,19] In order to implement the lowest noise flow setup the system is operated in open flow mode (siphon principle) and small flow rates of <0.1 mL min^{-1} are used. Sample solutions were stored in separate vessels and injected into the axial flow cell *via* a 6-way selection valve (Upchurch Scientific).

Sample preparation. Quartz crystal sensors were immersed in a modified piranha solution (1 : 2 H_2O_2(30%) : H_2SO_4) at 120 °C for 9 min. The crystals were then copiously rinsed with Milli-Q water for 5 min and dried in a stream of argon.

Safety note: Piranha solution is extremely aggressive and should be handled with care!

QCM measurements. Individual GSH adsorption measurements began with a flow of solvent (EtOH) over the QCM crystal surface. After a stable frequency baseline was reached (after about 1 h) GSH in solution (0.33 mM) was injected into the axial flow cell. Frequency measurements were performed with a 10 s gate time providing a frequency resolution of 0.01 Hz. The frequency shift was fitted to adsorption models within the Langmuir frame as detailed in the Appendix.

Results

The time-dependence of two prominent GSH signals obtained by ATR-IR measurements is depicted in Fig. 1. A detailed

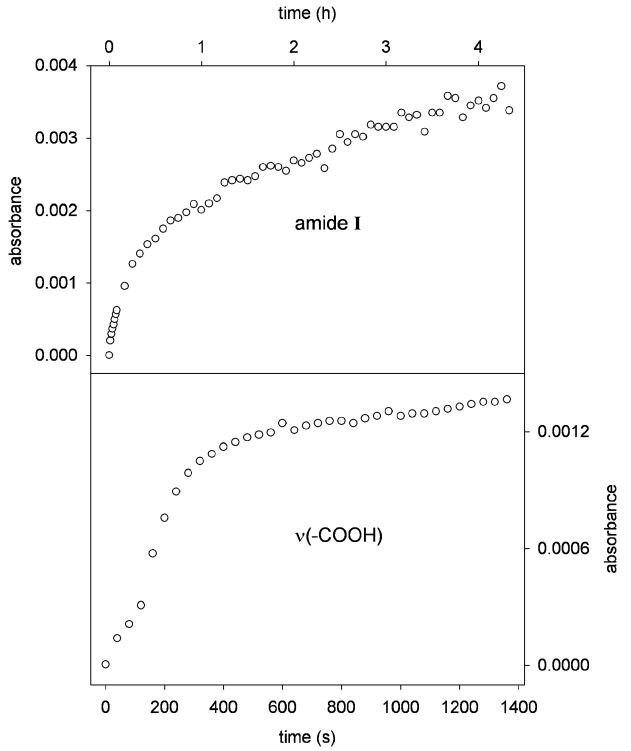

Fig. 1 Time-dependence of two prominent GSH signals obtained by ATR-IR when flowing (flow rate = 0.5 mL min^{-1}) GSH in solution (0.33 mM) over the gold coated Ge IRE. The absorbance as a function of time for the amide I signal and the ν(–COOH) signal is depicted in the upper and lower halves of this figure, respectively. Note that the two signals refer to the same GSH self-assembly process and each of the two signals is assigned a different time axis with the one for the amide I signal depicted above the upper graph.

assignment of the GSH infrared signals can be found elsewhere[12] but a summary of the most prominent bands is listed in Table 1. The absorbance as a function of time of the amide I signal at 1649 cm^{-1} is depicted in the upper half of Fig. 1 whereas the ν(–COOH) signal at 1731 cm^{-1} is displayed in the lower half. Due to their completely different behavior with time the signals are assigned a different time axis. The amide I signal shows a slow increase in intensity over a long time. In contrast, the intensity of the ν(–COOH) signal reveals a completely different behavior and almost stagnates in less than 1400 s. The completely different shape of the two curves in Fig. 1 shows that the ATR-IR spectrum is not only changing quantitatively but also qualitatively. Therefore, not only a bare mass uptake is observed in the ATR-IR experiment. The behavior shown in Fig. 1 points to other processes occurring simultaneously to adsorption and which affect the adsorbate spectrum qualitatively. This points to some structural changes during the self-assembly process, as will be discussed later.

Table 1 Observed vibrational bands of GSH depicted in the spectra in Fig. 4 and 5

GSH (zwitterionic)/cm^{-1}	Assignment
1731	ν(–COOH)
1649	Amide I
1600	ν_{as}(–COO^-)
1527	Amide II
1397	ν_s(–COO^-)
1230	δ(–C–O–H) bending + ν(–C–O) stretching

Diffusion can significantly influence the observed adsorption behavior at small bulk concentrations and/or high adsorption rates. In a non-stagnant liquid the thickness of the diffusion layer depends on the flow velocity. For two flow velocities $v_1 > v_2$ the thickness l of the diffusion layer becomes larger for smaller velocities, *i.e.* $l_2 > l_1$.[20] In order to estimate the influence of diffusion, experiments were repeated using flow rates of 0.18, 0.5, 1.0 and 1.25 mL min^{-1}. In further experiments GSH bulk concentrations of down to 0.04 mM were used, but in all these experiments the shape of the curves in Fig. 1 was not affected. It is therefore concluded that diffusion of GSH bulk molecules through the stagnant layer to the gold surface does not influence the adsorption behavior in our system.

The result of GSH adsorption on gold (solid line) as investigated by QCM is depicted in Fig. 2. Also given (dashed line) is a fit to a simple Langmuir (1L) model (see eqn (3) of the Appendix). Obviously, the shift in resonant frequency with time does not follow simple Langmuir (1L) kinetics. A more complex process with three different kinetic regimes is apparent. At the beginning of GSH adsorption, a sharp linear decrease in frequency is observed. This initial process is replaced after about 200 s by a slower, almost linear shift in resonant frequency. Finally, after about 1000 s, the onset of a very slow process is visible. This final step of the GSH adsorption process is still proceeding after 4000 s and a further shift (decrease) in frequency may fall below the detection limit. According to the Sauerbrey relation[14], assuming a mass sensitivity constant of 17.7 ng cm^{-2} Hz^{-1}, a frequency shift of 8.5 Hz (about saturation coverage) corresponds to 4.9×10^{-10} mol GSH cm^{-2}. This value should however only be taken as rough estimate considering the difficulty of determining absolute coverage by QCM in the liquid phase.[21] It should

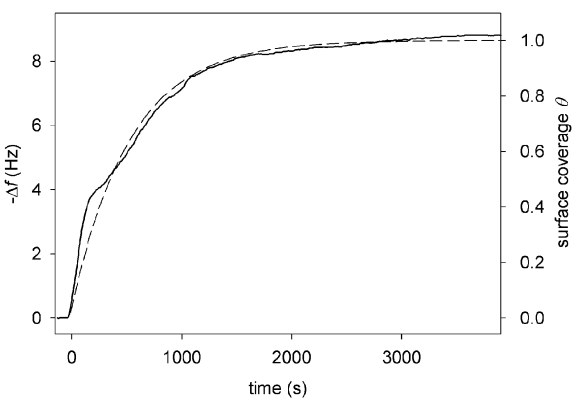

Fig. 2 The shift in resonance frequency upon GSH (0.33 mM) adsorption on gold as a function of time investigated by QCM (solid line). The flow rate was adjusted to 0.1 mL min^{-1} and the onset of GSH adsorption was taken as time zero. A Langmuir model (1L, see Appendix) was used to fit the data (dashed line).

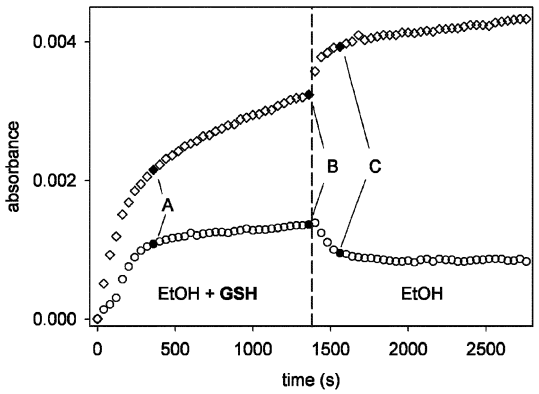

Fig. 3 The absorbance as a function of time for the amide I signal (diamonds) and the ν(–COOH) signal (circles). On the left-hand side, indicated by "EtOH + GSH", GSH in solution was flowed (flow rate = 0.5 mL min^{-1}) over the gold coated Ge IRE and replaced after 1380 s by an inflow of EtOH as indicated by "EtOH" on the right-hand side of this figure. Black circles and diamonds labelled with the letters A, B and C represent selected spectra which are displayed in Fig. 4 and 5.

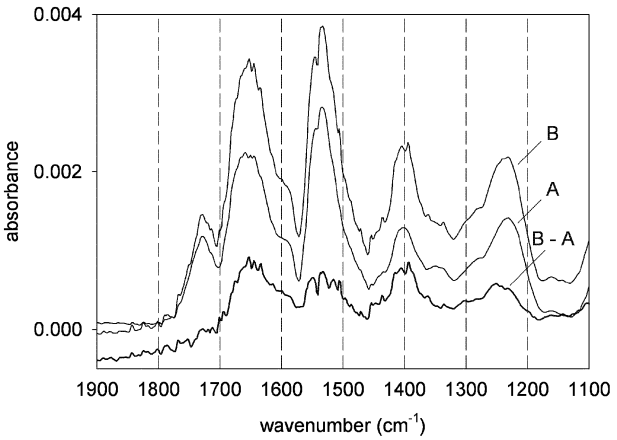

Fig. 4 GSH ATR-IR spectra recorded while flowing GSH in solution (0.33 mM, flow rate = 0.5 mL min^{-1}) over the gold coated Ge IRE. The spectrum labelled (A) was recorded 360 s after initial GSH self-assembly on gold (note that this spectrum refers to the first black circle/diamond indicated by A in Fig. 3). The spectrum (B) was recorded after 1360 s, just before the inflow of EtOH over the GSH SAM set in (see also Fig. 3). The corresponding difference spectrum B − A is also shown.

be noted that the described overall shape of the frequency shift curve was reproducible.

As already mentioned in the Experimental, an abrupt stop of GSH supply may have an impact on the GSH SAM structure. The spectral response to this stimulation is depicted in Fig. 3 where the absorbance as a function of time is displayed both for the amide I signal (represented as diamonds, upper plot) and the ν(–COOH) signal (circles, lower plot). For the left-hand side of Fig. 3, indicated by "EtOH + GSH", GSH in solution (0.33 mM) was flowed at 0.5 mL min^{-1} over the gold coated Ge IRE and GSH self-assembly took place. After 1380 s the supply of GSH molecules was stopped by flowing neat solvent (EtOH) at the same flow rate (0.5 mL min^{-1}) over the GSH SAM (right-hand side of Fig. 3, indicated by "EtOH"). The observed response of the amide I signals to EtOH flow over the GSH SAM is the opposite of that seen for ν(–COOH), as shown in the right-hand side of Fig. 3, which shows that the spectral changes can not be explained simply by desorption of weakly bound (physisorbed) molecules. This was further confirmed by analogous QCM experiments, which did not show a positive frequency shift upon flowing neat EtOH, as would be expected for desorption. Note that the response to the stimulation is occurring quickly. At about 120 s after the inflow of EtOH the ν(–COOH) signal has collapsed and reached a steady level whereas the amide I signal increases further, although at a slower rate. Careful inspection of the time-dependence of the two signals shows that the amide I signal increases slightly before the ν(–COOH) signal starts to decrease. In summary, Fig. 3, together with the result from the analogous QCM experiment, indicate that a reorganization within the adsorbate layer takes place upon flowing solvent, as will be discussed in detail later, and that desorption of weakly bound (physisorbed) molecules is only of minor importance for the observed spectral changes.

In order to gain more insight into the structural changes during adsorption and the flow of neat solvent, as indicated by the signals in Fig. 3, selected spectra (labelled by letters in Fig. 3) are depicted in Fig. 4 and 5, respectively. The first GSH spectrum shown was recorded 360 s after the inflow of GSH solution over the gold coated Ge IRE. This spectrum, labelled

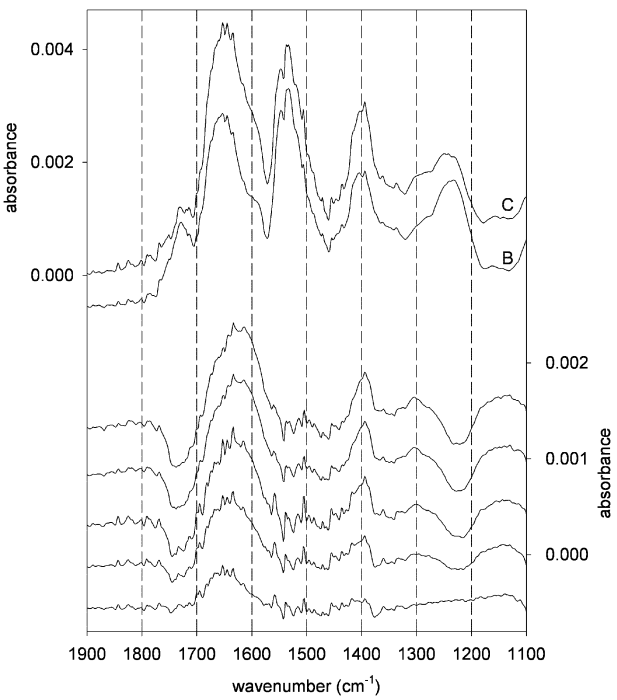

Fig. 5 The GSH absorption spectrum recorded before the EtOH inflow (flow rate = 0.5 mL min^{-1}) over the GSH SAM (B) is depicted in the upper half (note that this spectrum is identical to the one displayed in Fig 4). The spectrum recorded 200 s after the EtOH inflow (C) (third black circle/diamond C in Fig. 3) is also shown in the upper half. In the lower half a set of time-resolved difference spectra is shown which were obtained by subtracting the spectrum recorded at 1360 s (spectrum (B) in the upper half of this figure) from the five subsequent spectra. Time increases in intervals of 40 s from bottom to top.

(A) in Fig. 4, represents the adsorbate layer at the end of the initial fast adsorption process. In order of increasing intensity, three prominent GSH bands are visible at 1731 (ν(–COOH)), 1649 (amide I) and 1527 cm^{-1} (amide II). Less intense signals are apparent at 1397 (ν_s(–COO^-)) and 1230 cm^{-1} (δ(–C–O–H) bending + ν(–C–O) stretching). Spectrum (B) in Fig. 4 was recorded after 1360 s of GSH adsorption on the gold coated Ge IRE. The GSH coverage is now very large, *i.e.* adsorption is almost complete. All of the prominent GSH bands have gained intensity with the exception of the ν(–COOH) signal at 1731 cm^{-1}. The difference between the spectra recorded at 1360 (B) and 360 s (A) (see Fig. 3) is displayed in Fig. 4 (labelled B − A). Note that this difference spectrum reveals the changes associated with the final stages of SAM formation. Obviously, the ν(–COOH) signal at 1731 cm^{-1} is hardly apparent in the difference spectrum. All the other prominent GSH bands gained intensity, especially the amide I band at 1649 cm^{-1}.

The spectral response to solvent flow over the GSH adsorbate layer is depicted in Fig. 5. The spectrum recorded after 1360 s of GSH adsorption (B) is displayed in the upper half of Fig. 5 (the same spectrum is depicted in Fig. 4). It represents the final spectrum recorded before GSH in solution was replaced by EtOH. The second spectrum depicted in the upper half of Fig. 5 (C) was recorded 200 s after the EtOH inflow (see also Fig. 3). As can be expected from the time-dependence in Fig. 3 the ν(–COOH) signal at 1731 cm^{-1} has lost intensity and the amide I signal clearly appears more intense. Furthermore, the asymmetric band mainly associated with the amide I vibration has broadened in the region of 1600 cm^{-1}. In addition, the intensity of the band at about 1400 cm^{-1} has increased considerably compared to the two prominent GSH signals at 1527 and 1230 cm^{-1}. Difference spectra are shown in the lower half of Fig. 5 that were obtained by subtracting the spectrum recorded before GSH was replaced by EtOH (trace (B) in the upper half of Fig. 5) from the five subsequent spectra (the last spectrum in this set is labelled (C) in the upper half of Fig. 5). Time increases in intervals of 40 s (bottom to top), providing a temporal evolution of the processes occurring within the adsorbate layer. At 40 s after the onset of EtOH flow over the GSH SAM the amide I signal at 1649 cm^{-1} is clearly visible. Another small signal may be located at 1397 cm^{-1}. Obviously, the ν(–COOH) signal at 1731 cm^{-1} does not appear in this spectrum. Note that this behavior also emerges from Fig. 3, which shows that the amide I signal increases slightly before the ν(–COOH) signal starts to decrease. In the second difference spectrum (referring to 80 s after switching to EtOH flow over the GSH SAM) a negative band at 1731 cm^{-1} is visible due to a decrease in intensity of the ν(–COOH) signal. Simultaneously, the band at 1230 cm^{-1} associated with a carboxylic acid group (δ(–C–O–H) + ν(–C–O)) decreases as well. The amide I signal has gained further intensity, with a shoulder appearing at about 1600 cm^{-1}, which we assign to ν_{as}(–COO^-). The band at 1397 cm^{-1}, assignable to ν_s(−COO^-), is more pronounced as well. In the three subsequent difference spectra the discussed signals gain and lose intensity, respectively. Notably, the amide I band shifts to slightly lower wavenumbers which is due to the increase of the shoulder at 1600 cm^{-1}, assignable to ν_{as}(−COO^-). In summary, the set of time-resolved difference spectra reveals that upon flowing EtOH over the GSH SAM, processes with distinctly different kinetics take place, which are most apparent from the amide I and ν(–COOH) signals.

Discussion

The intensity of a signal in ATR-IR depends not only on the concentration or coverage of a surfaces species, but also on the transition dipole moment vector associated with the corresponding vibration and on the angle between the transition dipole moment vector and the electric field vector,[22,23] the latter being polarized perpendicular to metal surfaces.[24] Processes that affect these parameters thus influence the (relative) intensity of vibrational bands. The magnitude (and orientation) of the transition dipole moment of a vibration can be influenced by a change of the chemical entity (conformational changes, protonation/deprotonation *etc.*), whereas a change of the orientation of an adsorbed molecule will affect the angle between the transition dipole moment and the electric field. Fig. 1 reveals that the amide I and ν(–COOH) vibrational bands grow at different rates during adsorption and self-assembling of GSH on gold. The different time-dependence of the GSH ATR-IR signals thus strongly indicates structural changes within the adsorbate layer during self-assembly and shows that the ATR-IR signals do not only reflect mass uptake in this case. Using the benefits of a flow-through cell by changing the flow conditions and using considerably different GSH concentrations, it was further elucidated that the ATR-IR signals were not affected by diffusion effects.

As the ATR-IR signals measured during adsorption do not only represent the mass uptake, a second method, QCM, was used to shed some more light on the adsorption kinetics. Note that QCM was previously used to study the adsorption kinetics of thiols on gold.[21,25] The change (*i.e.* decrease) in resonant frequency depends on mass loading according to the Sauerbrey equation.[14] In liquid contact measurements, however, frequency changes may be affected by other factors. During SAM formation, the energy of the interaction of the surface with the solvent is changing.[25] In addition, viscous coupling of the liquid medium to the oscillating crystal surface results not only in a decrease in the resonant frequency but also in a damping of the resonant oscillation—the viscous loss is manifested as an increase in the resonance resistance R of the QCM resonator.[26] However, the measured frequency change during adsorption caused by these different processes is still assumed to be a direct result of the formation of the GSH SAM.[21] Because of the use of small GSH concentrations (0.33 mM) we assume that viscosity effects have a negligible influence on frequency measurements. The validity of this assumption was confirmed by the absence of a sharp increase in resonance resistance during the GSH self-assembling process.

The QCM data provide a complex picture of the GSH self-assembling process as is obvious by the different kinetic regimes. From Fig. 2 it emerges that the adsorption is fast up to a relative coverage of about 0.4 (assuming that the frequency shift is proportional to mass uptake and described by the 1L model). It is likely that at this point the adsorbed

molecules start to interact with each other. One possible explanation for the abrupt change in slope of the adsorption curve is a crossing of a phase boundary at this point. The structural changes during the self-assembly process as indicated by ATR-IR are thus further confirmed by the QCM measurements, which show a rather complex frequency shift with different slopes due to GSH adsorption. In other words, both the ATR-IR and QCM measurements coherently indicate structural changes within the adsorbate layer during self-assembly.

In principle, both the ATR-IR and QCM measurements are sensitive to the presence of physisorbed GSH at the SAM interface. However, two observations indicate that both the ATR-IR and QCM signals are dominated by chemisorbed species: First, the inflow of EtOH over the GSH modified QCM sensor crystals did not reveal a positive frequency shift as would be expected in case of the desorption of a weakly bound physisorbed species. Second, in the ATR-IR experiment the signals are expected to decrease upon desorption of physisorbed species. As is visible from Fig. 3 the amide I band is increasing upon switching to neat solvent (whereas the ν(–COOH) band decreases). This shows that upon changing to neat solvent structural changes within the adsorbate layer dominate the ATR-IR spectra over desorption of weakly bound (physisorbed) species.

The nature of the structural changes during self-assembly is addressed in the following. In order to extract information at the molecular level from the ATR-IR spectra, an assignment of the vibrational bands is required. A detailed discussion can be found elsewhere[12] and a summary of the most prominent bands observed in Fig. 4 and 5 is given in Table 1. In EtOH GSH exists in zwitterionic form with the acid group on the Glu moiety deprotonated and the one on the Gly protonated. Note that the stronger acid at the Glu protonates the amine (also at the Glu, see Scheme 1). We have recently shown that within a GSH SAM on gold a fraction of the adsorbed molecules are also deprotonated at the acid group of the Gly moiety.[12] This deprotonation is assisted by the interaction of the carboxylate group with the gold surface.

The ATR-IR signals revealing deprotonation/protonation of the acid groups are the ν(–COOH), $\nu_{as}(-COO^-)$ and $\nu_s(-COO^-)$ signals at 1731, about 1600 and 1397 cm^{-1}, respectively. The ν(–COOH) signal is most informative since it is associated with the protonated acid group of the Gly[12] and the corresponding band is well isolated in the spectrum. The carboxylate ($–COO^-$) bands are partly overlapped by other signals and furthermore associated with both the Gly and the Glu of the adsorbed GSH.

During the adsorption process the ν(–COOH) signal at 1731 cm^{-1} increases quickly until about 300 s before changing to a much more slowly increasing rate (Fig. 1 and 3). QCM and ATR-IR measurements reveal that after 300 s the surface is not yet fully covered. This shows that at relatively high coverage (*i.e.* after 300 s of adsorption) the increase of protonated acid groups on the surface through adsorption is compensated by a decrease through deprotonation. The protonated and deprotonated states at the acid group of the Gly co-exist on the surface in a dynamic equilibrium which can be shifted by changing the stability of one of the two states involved in the equilibrium. During the adsorption, at increasing coverage, intermolecular interactions may have an influence on the protonated (not surface bound)–deprotonated (surface bound) equilibrium of adsorbed molecules, thereby shifting the latter towards a new value. The ν(–COOH) signal in Fig. 1 indicates such a behavior. At high coverage the equilibrium shifts towards the deprotonated state, possibly due to intermolecular interactions.

The equilibrium between the protonated and deprotonated state of the acid group of the Gly moiety can also be shifted by the presence of dissolved GSH molecules. One possible reason is the stabilization of the protonated state due to hydrogen bonding of the protonated carboxylic acid group (a hydrogen bond donor) with dissolved molecules. Upon flowing EtOH, *i.e.* upon removing dissolved GSH, the ν(–COOH) signal collapses quickly (Fig. 3, circles) and simultaneously the bands associated with carboxylate vibrations, *i.e.* the $\nu_{as}(–COO^-)$ at 1600 cm^{-1} and the $\nu_s(–COO^-)$ at 1397 cm^{-1}, respectively, increase, as the time-resolved difference spectra in Fig. 5 reveal. Broad bands were also observed above 3000 cm^{-1} (not shown) upon flowing EtOH, which could partly be due to the O–H of the acid group but also due to the (reorientation of the) N–H groups or due to EtOH. The presence of dissolved GSH shifts the equilibrium towards the protonated state, whereas the presence of neat EtOH shifts the equilibrium towards the deprotonated state. It should be noted that readmission of GSH in solution shifts the equilibrium back towards the protonated state. Fig. 3 also shows that the amide I signal (diamonds, upper plot) keeps increasing in the absence of GSH, although at a considerably slower rate. This increase, which can not be due to adsorption, indicates that further slow structural changes proceed in the absence of GSH in solution, which do not affect the ν(–COOH) signal, since the latter stays constant.

The spectra recorded during the switching from GSH solution to neat EtOH solvent (Fig. 5) change not only quantitatively, but also qualitatively, showing that processes with different kinetics are responsible for the observed spectral changes. In particular, the amide I band at 1649 cm^{-1} starts to increase first (lower spectrum of Fig. 5). Only after some time, due to a deprotonation, the ν(–COOH) band at 1731 cm^{-1} loses intensity, *i.e.* becomes negative in the difference spectra in Fig. 5 and the carboxylate bands become positive. This means that before the deprotonation another process occurs, which leads to an increase of the amide I signal. Such a sudden increase of the amide I band intensity can be induced by a reorientation of the amide group(s) of adsorbed GSH. This reorientation is characterized by an alignment of the corresponding transition dipole moment to be more parallel to the electric field, the latter being oriented perpendicular to the surface. Such an alignment would result in a stronger ATR signal. Note that due to the metal surface selection rule[24] only the component of the transition dipole moment normal to the metal surface gives rise to IR intensity.

Based on the spectral features just discussed and relying on former findings on the GSH–gold system,[12] which revealed that the acid group of the Glu moiety of GSH is deprotonated, whereas part of the GSH molecules are protonated at the Gly part of the molecule, we propose that a large fraction of GSH

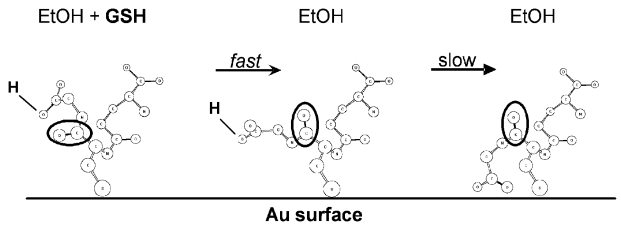

Fig. 6 Pictorial representation of the suggested structural change that a large fraction of the adsorbed GSH molecules undergoes by removing dissolved GSH from the SAM interface. The initial state is depicted on the left. In a fast step the reorganization of the Gly part of the molecule changes the orientation of the strong amide I transition dipole moment (compared to that depicted on the left) as can be seen in the intermediate picture. Note that at this stage a large fraction of the acid groups of the Gly moiety is still protonated. In the subsequent slower step the Gly acid groups are deprotonated by interaction with the gold surface (right).

molecules within the SAM undergo the following structural changes by admitting EtOH, *i.e.* removing dissolved GSH from the SAM interface (see Fig. 6): In an initial fast step the interfacial interactions between the acid groups of the Gly part of the adsorbed GSH molecules and dissolved GSH molecules are lost by the removal of the latter. This loss in interaction induces reorganization to a new energetically favorable state. As discussed above, this state is found upon deprotonation of the corresponding acid group by interaction with the Au surface. This new state is reached in two steps with distinctly different kinetics. In a first step, a reorientation of the Gly part of the molecule (see Fig. 6, centre) takes place. This increases the alignment of the strong amide I transition dipole moment with the electric field, the latter being perpendicular to the surface (compared to the initial state represented by Fig. 6, left), leading to the observed increase of the amide I signal. In the following second step the Gly acid groups now interact with the Au surface and deprotonate as depicted in Fig. 6, right. The involved deprotonation thus becomes visible in the absorbance spectra as the decreasing ν(–COOH) band at 1731 cm^{-1}. At this point it should be noted that GSH involves two amide groups (the Gly and Glu of the molecule). Though structural changes are likely to occur in the Glu part of the molecule as well, we assume that the major contribution to the increase in the amide I signal while flowing EtOH over the GSH SAM is attributable to the amide group of the Gly arm of the molecule since this arm finally interacts with the gold surface *via* the carboxylate.[12] In contrast, during the adsorption process the slow increase of the amide I band at 1649 cm^{-1} is not specifically attributable to the Gly or Glu moieties.

Conclusions

Both the ATR-IR and QCM results show that GSH adsorption on gold is a complex process involving distinctly different kinetic regimes depending on surface coverage. This leads to mass uptake curves in the QCM experiments that are far from being smooth as would be the case for simple Langmuir adsorption. In ATR-IR this behavior is reflected by the different time-dependence of the bands in the spectra, notably the amide I and ν(–COOH) bands. The latter band increases significantly only in the beginning of adsorption, when QCM reveals very fast mass uptake and remains almost constant in intensity afterwards. In contrast, the amide I signal keeps increasing at appreciable rate for a much longer time. Experiments performed at different flow rates and concentrations clearly show that adsorption is not diffusion-limited under the applied conditions. The spectroscopic results point to a structural change within the adsorbate layer, which is overlaid by the adsorption process. The clear distinction of several kinetic regimes observed by both of the applied techniques strongly indicates that the structure of the adsorbate layer is coverage dependent, leading to crossings of phase boundaries of the phase diagram as coverage is increasing during adsorption. A dominant role for the relevant structural changes is played by the acid group of the Gly moiety of GSH, which is protonated when dissolved in ethanol, but partly deprotonated when adsorbed, assisted by the interaction of the corresponding carboxylate group with the surface. The deprotonated state becomes more favored at coverages where intermolecular interactions cannot be neglected. It is further evident from the experimental results that the equilibrium between protonated and deprotonated states is easily shifted by external stimuli, such as the presence of dissolved GSH. Upon removal of dissolved GSH the relaxation of the system towards the new equilibrium state is fast, but proceeds in at least two distinct steps with different kinetics. Based on the ATR-IR measurements a model for the structural change is provided.

Appendix

The QCM data was fit to the well known first order Langmuir model (1L), which assumes that the surface reaction rate is proportional to the number of available sites for adsorption according to

$$\frac{\mathrm{d}\theta}{\mathrm{d}t} = k_{\mathrm{ads}} c(1-\theta) - k_{\mathrm{des}}\theta \qquad (1)$$

where θ denotes the fractional surface coverage, c is the bulk concentration of dissolved molecules and k_{ads} and k_{des} are the rate constants for adsorption and desorption, respectively. Integrating eqn (1) with respect to time t gives the following analytical expression for $\theta(t)$:

$$\theta(t) = \left(1 + \frac{k_{\mathrm{des}}}{k_{\mathrm{ads}}}\frac{1}{c}\right)^{-1} \{1 - \exp(-(k_{\mathrm{ads}}c + k_{\mathrm{des}})t)\} \qquad (2)$$

Assuming $k_{\mathrm{des}} \approx 0$ for thiol adsorption eqn (2) further simplifies to

$$\theta(t) = 1 - \exp(-k_{\mathrm{ads,1L}}ct) \qquad (3)$$

In order to fit the QCM data, eqn (3) was modified according to

$$A(t) = A_\infty \{1 - \exp(-k_{\mathrm{ads,1L}}ct^b)\} \qquad (4)$$

where the exponent $b = 1$ for the 1L adsorption model. $A(t)$ is the measured signal, *i.e.* frequency shift for QCM. In eqn (4) the factor A_∞ and rate constant $k_{\mathrm{ads,1L}}$ are fittable parameters. Note that for $t \to \infty$ $A(t) \to A_\infty$ and the ratio $A(t)/A_\infty \leq 1$ thus represents the fractional surface coverage $\theta(t)$.

Acknowledgements

Financial support from the Swiss National Science Foundation is gratefully acknowledged. The use of the sputtering facilities at the Swiss Center for Electronics and Microtechnology in Neuchâtel (CSEM) is acknowledged.

References

1 C. D. Bain and G. M. Whitesides, *Science*, 1988, **240**, 62.
2 A. Ulman, *Chem. Rev*., 1996, **96**, 1533.
3 F. Schreiber, *J. Phys.: Condens. Matter*, 2004, **16**, R881.
4 R. Jelinek and S. Kolusheva, *Chem. Rev*., 2004, **104**, 5987.
5 G. E. Poirier, *Langmuir*, 1999, **15**, 1167.
6 M. O. Lorenzo, C. J. Baddeley, C. Muryn and R. Raval, *Nature*, 2000, **404**, 376.
7 E. M. Marti, C. Methivier and C. M. Pradier, *Langmuir*, 2004, **20**, 10223.
8 H. Sies, *Free Radical Biol. Med*., 1999, **27**, 916.
9 S. Kanagaraja, S. Alaeddine, C. Eriksson, J. Lausmaa, P. Tengvall, A. Wennerberg and H. Nygren, *J. Biomed. Mater. Res*., 1999, **46**, 582.
10 M. Hepel and E. Tewksbury, *J. Electroanal. Chem*., 2003, **552**, 291.
11 K. Takehara, M. Aihara and N. Ueda, *Electroanalysis*, 1994, **6**, 1083.
12 M. Bieri and T. Bürgi, *Langmuir*, 2005, **21**, 1354.
13 N. J. Harrick, *Internal Reflection Spectroscopy*, Interscience Publishers, New York, 1967.
14 G. Sauerbrey, *Z. Phys*., 1959, **155**, 206.
15 B. El Roustom, G. Foti and C. Comninellis, *Electrochem. Commun*., 2005, **7**, 398.
16 A. Urakawa, R. Wirz, T. Bürgi and A. Baiker, *J. Phys. Chem. B*, 2003, **107**, 13061.
17 T. Bürgi and A. Baiker, *J. Phys. Chem. B*, 2002, **106**, 10649.
18 T. Dabros and T. G. M. van de Ven, *Phys. Chem. Hydrodyn*., 1987, **8**, 161.
19 T. Dabros and T. G. M. van de Ven, *Colloid Polym. Sci*., 1983, **261**, 694.
20 U. P. Fringeli, D. Baurecht and H. H. Günthard, in *Infrared and Raman Spectroscopy of Biological Materials*, ed. H. U. Gremlich and B. Yan, Marcel Dekker, Inc,, New York, 2000.
21 W. Pan, C. J. Durning and N. J. Turro, *Langmuir*, 1996, **12**, 4469.
22 H. Shinohara, T. Kasahara, K. Kadokura, Y. Uryu and K. Itoh, *J. Phys. Chem. B*, 2004, **108**, 3584.
23 S. C. Street and A. J. Gellman, *J. Chem. Phys*., 1996, **105**, 7158.
24 M. Osawa, K.-I. Ataka, K. Yoshii and T. Yotsuyanagi, *J. Electron Spectrosc. Relat. Phenom*., 1993, **64/65**, 371.
25 D. S. Karpovich and G. J. Blanchard, *Langmuir*, 1994, **10**, 3315.
26 K. K. Kanazawa and J. Gordon II, *Anal. Chem*., 1985, **57**, 1770.